NeuroImage: Clinical 32 (2021) 102831

Contents lists available at ScienceDirect

NeuroImage: Clinical

journal homepage: www.elsevier.com/locate/ynicl

Utility of quantitative susceptibility mapping and diffusion kurtosis imaging in the diagnosis of early Parkinson's disease

Samantha Tan [a,1], Septian Hartono [b,c,1], Thomas Welton [b,c], Chu Ning Ann [a,b], Soo Lee Lim [a,d], Tong San Koh [c,e], Huihua Li [a,c], Fiona Setiawan [b], Samuel Ng [b], Nicole Chia [b], Saifeng Liu [f], E. Mark Haacke [f,g], Eng King Tan [b,c], Louis Chew Seng Tan [b,c], Ling Ling Chan [a,c,*]

[a] Singapore General Hospital, Singapore, Singapore
[b] National Neuroscience Institute, Singapore, Singapore
[c] Duke-NUS Graduate Medical School, Singapore, Singapore
[d] National Heart Centre Singapore, Singapore, Singapore
[e] National Cancer Centre Singapore, Singapore, Singapore
[f] MRI Institute for Biomedical Research, Bingham Farms, MI, USA
[g] Wayne State University, Detroit, MI, USA

ARTICLE INFO

Keywords:
Parkinson disease
Iron overload
Diffusion magnetic resonance imaging
Substantia nigra
Basal ganglia

ABSTRACT

Objective: To investigate the utility of quantitative susceptibility mapping (QSM) and diffusion kurtosis imaging (DKI) as complementary tools in characterizing pathological changes in the deep grey nuclei in early Parkinson's disease (PD) and their clinical correlates to aid in diagnosis of PD.

Method: Patients with a diagnosis of PD made within a year and age-matched healthy controls were recruited. All participants underwent clinical evaluation using the Unified Parkinson's Disease Rating Scale (MDS-UPDRS III) and Hoehn & Yahr stage (H&Y), and brain 3 T MRI including QSM and DKI. Regions-of-interest (ROIs) in the caudate nucleus, putamen, globus pallidus, and medial and lateral substantia nigra (SN) were manually drawn to compare the mean susceptibility (representing iron deposition) and DKI indices (representing restricted water diffusion) between PD patients and healthy controls and in correlation with MDS-UPDRS III and H&Y, focusing on susceptibility value, mean diffusivity (MD) and mean kurtosis (MK).

Results: There were forty-seven PD patients (aged 68.7 years, 51% male, disease duration 0.78 years) and 16 healthy controls (aged 67.4 years, 63% male). Susceptibility value was increased in PD in all ROIs except the caudate, and was significantly different after multiple comparison correction in the putamen (PD: 64.75 ppb, HC: 44.61 ppb, $p = 0.004$). MD was significantly higher in PD in the lateral SN, putamen and caudate, the regions with the lowest susceptibility value. In PD patients, we found significant association between the MDS-UPDRS III score and susceptibility value in the putamen after correcting for age and sex ($\beta = 0.21$, $p = 0.003$). A composite DKI-QSM diagnostic marker based on these findings successfully differentiated the groups ($p < 0.0001$) and had "good" classification performance (AUC = 0.88).

Conclusions: QSM and DKI are complementary tools allowing a better understanding of the complex contribution of iron deposition and microstructural changes in the pathophysiology of PD.

Abbreviations: AC, Anterior commissures; AD, Axial diffusivity; AK, Axial kurtosis; BET, Brain extraction tool; DKE, Diffusional Kurtosis Estimator; DKI, Diffusion kurtosis imaging; DTI, Diffusion tensor imaging; EPI, Echo Planar Imaging; FA, Fractional anisotropy; FLAIR, Fluid-Attenuated Inversion Recovery; FMRIB, Functional MRI of the Brain; FOV, Field of view; FSL, FMRIB Standard Library; GP, Globus pallidus; H&Y, Hoehn and Yahr; HC, Healthy controls; ICC, Intraclass correlation coefficient; KFA, Kurtosis fractional anisotropy; MD, Mean diffusivity; MK, Mean kurtosis; MDS, Movement Disorder Society; MPRAGE, Magnetization-Prepared Rapid Acquisition with Gradient Echo; MRI, Magnetic Resonance Imaging; NINDS, National Institute of Neurological Disorders and Stroke; PC, Posterior commissures; PD, Parkinson's disease; QSM, Quantitative susceptibility mapping; RD, Radial diffusivity; RK, Radial kurtosis; ROI, Regions of interest; SE, Spin Echo; SHARP, Sophisticated harmonic artifact reduction for phase; SN, Substantia nigra; SRNCP, Sorting by reliability following a non-continuous path; TSVD, Truncated singular value decomposition; UPDRS, Unified Parkinson's Disease Rating Scale.

* Corresponding author at: Department of Diagnostic Radiology, Singapore General Hospital, Singapore, Outram Road, Singapore 169608, Singapore.
E-mail address: chan.ling.ling@singhealth.com.sg (L. Ling Chan).

[1] Samantha Tan and Septian Hartono contributed equally to this work.

https://doi.org/10.1016/j.nicl.2021.102831
Received 5 May 2021; Received in revised form 16 September 2021; Accepted 18 September 2021
Available online 22 September 2021

1. Introduction

Parkinson's disease (PD) is characterized by resting tremor, muscle rigidity, bradykinesia and postural instability. These symptoms are attributed to the loss of dopaminergic neurons in the substantia nigra (SN) and intraneuronal Lewy bodies, and progressively worsen with time (Damier et al., 1999). PD is diagnosed largely based on clinical discrimination, making it hard to detect early stages of the disease and hard to assess its severity compared with other causes of parkinsonism (Hughes et al., 2002).

Diffusion tensor imaging (DTI) has been used to assess features of parkinsonism as it is able to quantify microstructural damage through assessment of the diffusion properties of white matter. DTI is sensitive to degeneration in the substantia nigra (SN), corpus callosum, and the cingulate and temporal cortices in PD (Atkinson-Clement et al., 2017). DTI assumes that the diffusion of water molecules occurs in a free and unrestricted environment, and the diffusion displacement follows a Gaussian model. However, diffusion heterogeneity in biological tissues exists due to cellular barriers, complex water exchange and compartmentalization leading to the restriction of water and structural complexity (Basser and Jones, 2002; Lu et al., 2006). Hence, water molecular diffusion would deviate from random Brownian motion and follow a non-Gaussian distribution instead. Diffusion kurtosis imaging (DKI) accounts for this variation, providing a more accurate model to study non-Gaussian water diffusion in biological tissue (Steven et al., 2014). The heterogeneity and complexity of grey matter structures are reflected by increased kurtosis on DKI, and studies have shown that DKI is a more sensitive means for severity evaluation in PD (Wang et al., 2011; Zhang et al., 2015).

Iron plays an important role in numerous biological processes in the human brain such as DNA synthesis and myelination (Rouault, 2013). Although aberrant and excessive iron deposition found in post-mortem studies has been linked to the pathology and pathogenesis of many neurodegenerative diseases like PD (Griffiths and Crossman, 1993), high iron deposition in deep grey matter remains a nonspecific finding (Sian-Hülsmann et al., 2011). The exact role of iron in the pathogenesis of PD remains unclear. Nevertheless, iron deposition in the pars compacta of the substantia nigra parallels the loss of dopaminergic neurons (Dusek et al., 2012; Dusek et al., 2015). Quantitative susceptibility mapping (QSM) is an MR imaging technique that has been used to evaluate PD (Ghassaban et al., 2019a). QSM allows for non-invasive quantification of iron deposition in tissues through measurement of relative magnetic susceptibility in the tissue. It identifies differences in iron, calcification and myelin in diseased and healthy brain tissues (Langkammer et al., 2012; Wang and Liu, 2015) and is potentially better than conventional T2-weighted and T2*-weighted sequences which lack specificity in characterizing histopathological events in the deep grey matter (Alkemade et al., 2017). A number of QSM studies have found higher magnetic susceptibility in the red nucleus and substantia nigra of PD patients than healthy controls (Barbosa et al., 2015; Azuma et al., 2016). Recently, one study has shown that those patients with the highest iron content also have higher Movement Disorder Society Unified Parkinson's Disease Rating Scale (MDS-UPDRS) scores (Ghassaban et al., 2019b; Sethi et al., 2019). The combination of DKI and QSM may be useful for the diagnosis of neurological disease as DKI can interrogate the microstructural complexity of tissue while QSM is sensitive to changes in local susceptibility due to the presence of diamagnetic (calcium) and paramagnetic (iron) materials (Welton et al., 2019).

In this study, we investigated the utility of QSM and DKI as complementary tools in characterizing pathological changes in deep grey nuclei in early PD and their clinical correlates. We hypothesized that, in the basal ganglia of patients with PD relative to healthy controls, that iron concentration would be higher, diffusivity would be higher and kurtosis would be lower, and that a combined biomarker based on these measures would be sensitive to PD diagnosis.

2. Materials and methods

2.1. Subjects

This study was approved by the institutional ethics committee of SingHealth. Written consent was obtained from all study participants. Patients were recruited if they fulfilled the criteria for PD diagnosis as defined by the Advisory Council of the United States National Institute of Neurological Disorders and Stroke (Gelb et al., 1999). The PD diagnoses were made <1 year before recruitment, with the onset of cardinal motor symptoms occurring <2 years before diagnosis (Huang et al., 2019). Patients with PD plus syndromes, atypical Parkinsonism with a poor levodopa response and PD diagnoses changed after clinical follow-up of at least 3 years were excluded from this analysis. Healthy controls were volunteers of a similar age, without neurodegenerative diseases and examined by the investigators. All participants were English or Mandarin speaking and had the ability to read or write in English or Mandarin. Participants who were older than 90 years or younger than 21 years of age, with a history of clinical or symptomatic stroke, active malignancy, end-organ failure, significant orthopaedic abnormalities that affected movement and/or other significant neurological or psychiatric conditions were excluded. Motor subtyping was based on Stebbins' method using MDS-UPDRS part II and III (Stebbins et al., 2013). All participants underwent clinical motor evaluation using the MDS-UPDRS III and modified Hoehn and Yahr (H&Y) staging.

2.2. Brain MRI

MRI was performed on a 3.0 Tesla scanner (Skyra, Siemens Healthcare, Erlangen, Germany) with a 32-channel head coil. A three-dimensional whole brain multi-echo gradient recalled echo (GRE) T2*-weighted imaging sequence was acquired using the following parameters: TR = 53 ms, TE = 7.5/14.8/20/26.4 ms, FA = 15°, matrix = 256 × 192, slice thickness = 2 mm, FOV = 230 mm × 172 mm, resolution = 0.9 × 0.9 × 2 mm, acquisition time = 7:18.

DKI was acquired with a spin-echo echo planar imaging (SE-EPI) sequence using the following parameters: TR = 10118 ms, TE = 102 ms, FA = 90°, matrix = 122 × 122, slice thickness = 2.5 mm, FOV = 220 mm × 220 mm, resolution = 1.8 × 1.8 × 2.5 mm, acquisition time = 11:09, the same set of 30 diffusion-encoding directions each at b-values = 1000 and 2000 s/mm^2. Three non-diffusion-weighted volumes (b = 0) were also acquired, spaced uniformly in the acquisition to address signal drift.

We also performed a sagittal T1 MPRAGE (TR = 1900 ms, TE = 2.44 ms, TI = 900 ms, matrix = 256 × 256, slice thickness = 1 mm, FOV = 250 mm × 250 mm, resolution = 1 × 1 × 1 mm) and T2 FLAIR (TR = 7000 ms, TE = 132 ms, TI = 2210 ms, matrix = 256 × 256, slice thickness = 4 mm, FOV = 220 mm × 220 mm, resolution = 0.86 × 0.86 × 4 mm). All other sequences were acquired parallel to the anterior-posterior commissures (AC-PC).

2.3. DKI post-processing

Eddy current distortions were corrected with an affine intrasubject registration to the respective individual b_0 image by means of the eddy correction procedure implemented in FSL (Oxford Centre for Functional MRI of the Brain, Oxford, United Kingdom). DKI tensor estimation was done using Diffusional Kurtosis Estimator (DKE) 2.6 (Medical University of South Carolina, Charleston, SC) (Tabesh et al., 2011) which smoothed the data using the Gaussian kernel, rotated the b-matrix, masked background voxels, estimated the diffusion tensors and calculated the parameters. DKI parameter maps were co-registered using in-house software written in MATLAB (MathWorks, Natick, MA). Parameters obtained were mean, axial and radial diffusivity (MD, AD, RD), fractional anisotropy (FA), mean, axial and radial kurtosis (MK, AK, RK) and kurtosis fractional anisotropy (KFA).

2.4. QSM post-processing

QSM post-processing was performed using SPIN software (SpinTech Inc., Bingham Farms, USA). Channel-combined magnitude images were generated from the multichannel complex images by the root sum of squares of the multichannel magnitude images. Brain extraction based on magnitude images was performed using FSL Brain Extraction Tool (BET2). Phase images of different TEs were unwrapped using the 3D sorting by reliability following a non-continuous path (3D-SRNCP) algorithm. Background field phase was removed from the unwrapped phase images using a truncated singular value decomposition (TSVD) implementation of Sophisticated Harmonic Artifact Reduction for Phase data (SHARP). Regularized k-space inverse filtering was performed on the processed phase images to generate the initial QSM images. An iterative k-space algorithm was used on the initial QSM images to yield the final mean susceptibility (iron deposition) map (Barbosa et al., 2015; Haacke et al., 2010). QSM data are reported as parts per billion (ppb). Since free iron contributes minimally to the measured susceptibility value, the susceptibility value mainly refers to the iron that is bound with ferritin.

2.5. Image analysis

Regions-of-interest (ROIs) in the caudate, putamen, globus pallidus (GP), and medial and lateral SN were manually drawn by two independent raters (after rigorous intensive training) blinded to subject status on anatomically consistent sections, pre-selected after thorough radiological review of both DKI and QSM images across the cohort of both PD patients and controls, under supervision by a neuroradiologist with >20 years of practice and significant experience in SN ROI placement germane to PD. Rater 1 repeated ROI placement on a separate session 6 weeks later. The best slice that enabled the largest possible ROI placement for each grey nucleus and representative of the 3D nuclear structures was chosen for ROI placement bilaterally for all structures of interest (Fig. 1). The mean value was computed for each ROI.

For DKI, ROIs of the GP, putamen and caudate were drawn on the b0 maps on slices + 5 mm (2 slices), +7.5 mm (3 slices) and + 10 mm (4 slices) above that containing the AC-PC respectively. For QSM images, ROIs were drawn on best matching slices at + 4 mm (2 slices), +6mm (3 slices) and + 8 mm (4 slices) above the most superior cut containing the red nucleus (this cut also contained the AC-PC) respectively. These ROIs maximized the largest possible nuclear coverage along the boundaries of each structure, and were visually checked immediately against the FA maps to ensure that the ROI margins do not bleed into the cerebrospinal fluid and white matter in the adjacent lateral ventricular frontal horn and capsules respectively.

The margins of the smaller SN were less distinct on the DKI than QSM images, which precluded direct manual SN segmentation. Yet, reproducibility of ROI placement between the two raters on both sets of DKI and QSM images across the entire cohort containing PD patients and controls is important. The DKI and QSM slice for SN ROI placement was determined based on the best cut that afforded both consistent placement of two circular ROIs and identification of the anatomy. These were the slice immediately below the red nucleus for DKI images, and the most inferior slice where both the red nucleus and SN were visualized for QSM images. Circle ROIs with a diameter of 5.4 mm (as anatomically constrained by SN width), and divided into medial and lateral ROIs, were drawn to capture known spatial differences in degeneration (Vaillancourt et al., 2009) in the SN.

2.6. Statistical analysis

Statistical analyses were performed using R (version 3.4.2). Intra- and inter-rater reliability of the DTI/DKI and QSM values extracted from the ROIs was assessed by intraclass correlation coefficient (ICC). ROI measurements from Rater 1 was used for all analyses. Group demographics were compared using t-tests, and Chi-square tests. We analyzed MD and MK as the primary diffusion and kurtosis measures. FA, KFA, AD, RD, AK and RK were included as secondary outcomes. All variables were inspected to confirm normal distribution and the appropriate parametric or non-parametric test applied. Statistical significance was defined as $p < 0.05$. For each set of tests in the primary outcomes (susceptibility value, MD and MK), we corrected for multiple comparisons using the Bonferroni method (i.e., for 3 measures and 5 ROIs, $0.05/15 = 0.003$).

Independent samples t-tests were used to compare susceptibility

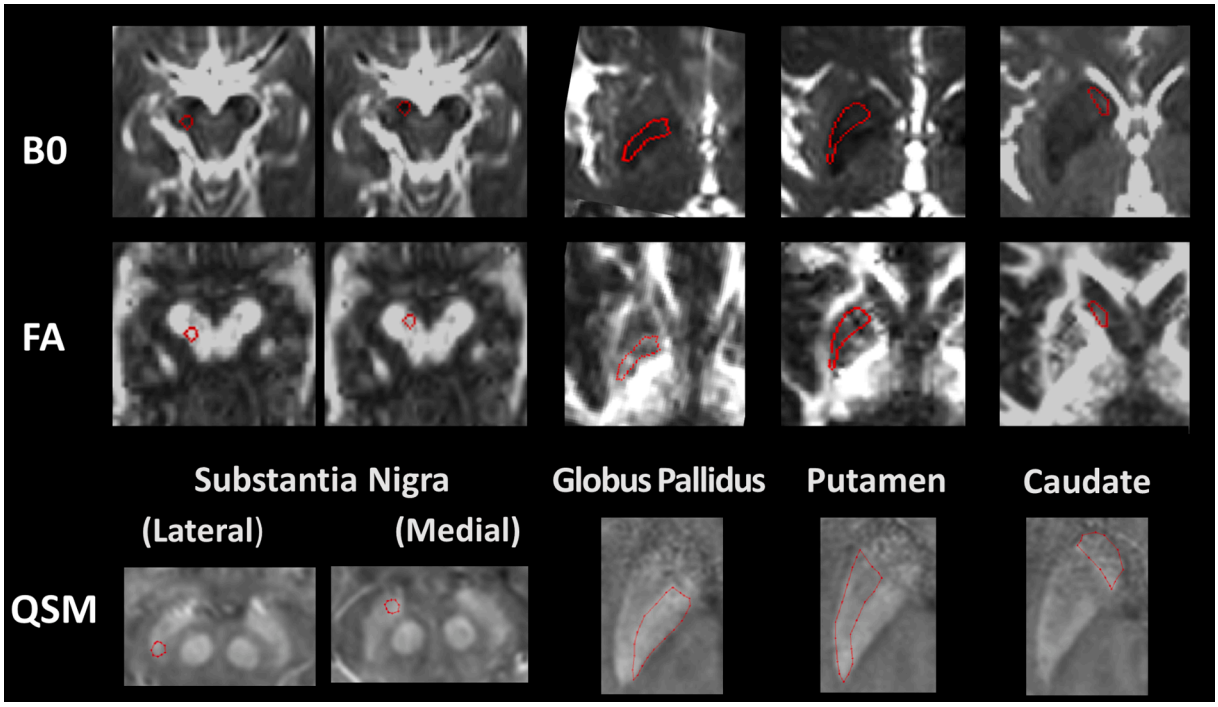

Fig. 1. ROI placement at the substantia nigra, globus pallidus, putamen and caudate on DKI B0 and FA maps, and QSM.

value and DKI indices between PD patients and HC. To test association of the primary imaging measures with clinical scores in the PD group, we performed linear regression controlling for age and sex for the MDS-UPDRS III and H&Y stage. Linear regression was performed between susceptibility value and MD/MK in each region, controlling for age and sex. For each regression, we reported the unstandardized β coefficient and 95% confidence intervals (CI). Normality of the residuals was confirmed for all regressions. Based on the findings, we formed a composite PD diagnostic DKI-QSM marker which combined the measures found with significant results in a simple formula. In a post-hoc analysis, the performance of this marker in discriminating PD and control groups was analyzed using the receiver operating characteristic curve.

3. Results

3.1. Sample characteristics

We included 47 early PD patients (24 males, mean age 68.7 years) and 16 healthy controls (10 males, mean age 67.4 years; Table 1). All patients were on medication and free from major cognitive impairment. There were no significant differences in age or gender between PD and HC groups. Twenty-eight of the PD patients were tremor dominant, 1 rigidity dominant, 14 bradykinesia dominant and 4 others. Review of the T2 FLAIR images by a neuroradiologist with >2 decades of experience revealed no visual differences in grey matter nuclei between PD patients and controls in terms of atrophy, iron deposition or gliosis. The intra-rater ICC was classed as "very good" (ICC > 0.85) for all QSM and DKI ROIs, while the inter-rater ICC was "very good" (ICC > 0.85) and "good" (ICC > 0.7) for all QSM and DKI ROIs respectively (Cicchetti, 1994).

3.2. Group differences in susceptibility value and diffusion kurtosis

There were no differences in ROI size between groups. In addition, there were no differences in ROI measurements between hemispheres, and therefore the ROI measurements were pooled across the hemispheres. We found overall elevated susceptibility value in the basal ganglia across all ROIs in PD patients compared to controls (Fig. 2; Table 2) except the caudate nucleus. We found a significant group difference in susceptibility value in the putamen (PD: 64.75 ppb, HC: 44.61 ppb, $p = 0.004$) which passed multiple comparison correction. In PD patients, the highest levels of iron were detected in the globus pallidus (133.71 ppb) and the medial SN (110.32 ppb). By comparison, the lateral SN (87.64 ppb) had much lower iron than the medial SN.

For the primary diffusion and kurtosis measures, we found a pattern of significantly increased MD in PD in all regions except the medial SN and GP, and of similar MK across all regions (Fig. 2; Table 3). The largest difference in MD was observed in the caudate, with the PD group having significantly higher MD that passed multiple comparison correction (PD: 1.16, HC: 0.96; $p < 0.001$). Inspection of differences in the secondary diffusion measures (Table S1) revealed that this MD difference was driven by an increase in the RD ($p < 0.001$), but not AD ($p = 0.426$). Caudate FA was also affected ($p = 0.015$) and elevated in PD due to the combination of increased RD and unchanged AD. No group difference in the caudate was reflected in the MK, but inspection of the secondary kurtosis measures revealed a lower KFA in PD ($p = 0.006$).

Table 1
Study demographics. Values are given as mean (SD). P-values are for a *t*-test or chi-square test (for sex).

Clinico-Demographics	PD	HC	T-value	P-value
Age, years	68.7 (8.3)	67.4 (6.4)	−0.55	0.587
Number	47	16		
Sex			0.63	0.428
Male	24 (51%)	10 (63%)		
Female	23 (49%)	6 (37%)		
H&Y	1.66 (0.48)	–		
MDS-UPDRS III	23.49 (9.86)	–		
Disease duration, years	0.78 (0.56)	–		

PD, Parkinson's Disease; HC, Healthy Controls; H&Y, Hoehn & Yahr stage; MDS-UPDRS III, Movement Disorder Society-Unified Parkinson's Disease Rating Scale Part III; SD, standard deviation.

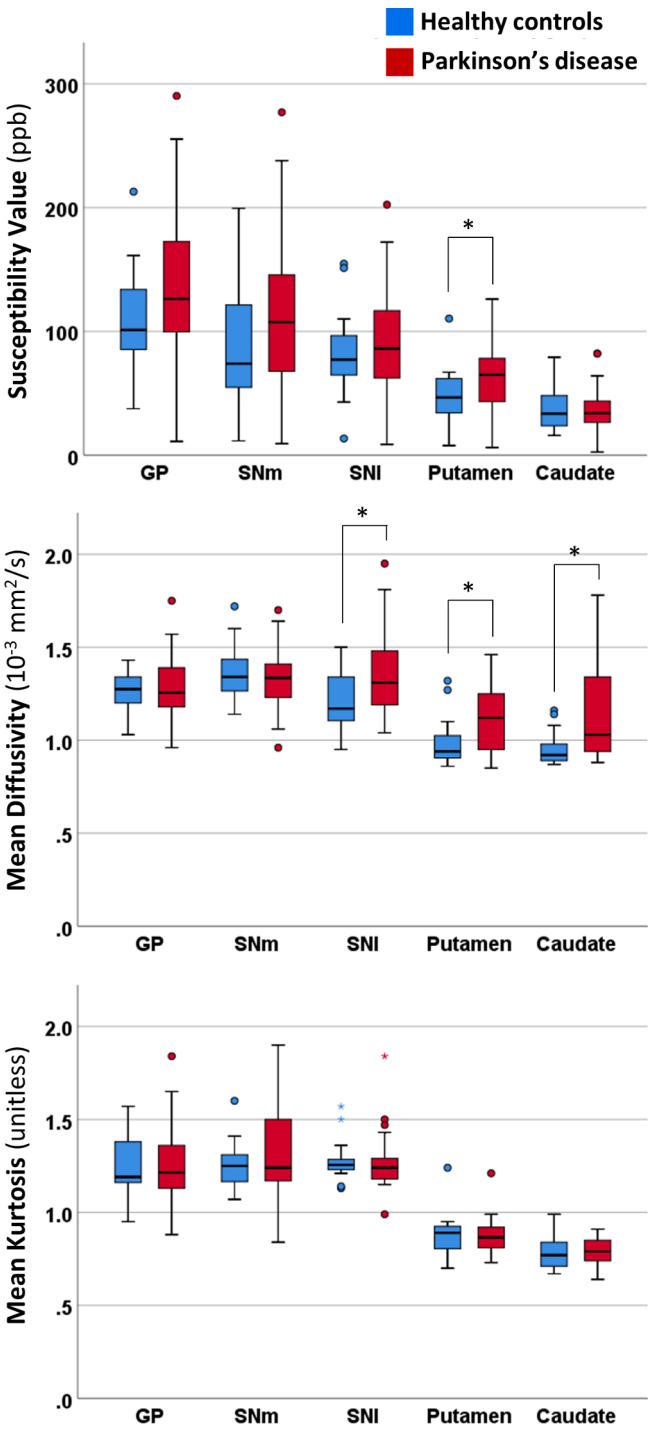

Fig. 2. Group differences in susceptibility value, and primary diffusion and kurtosis indices on QSM and DKI respectively in each region of interest. Looking horizontally, the iron deposition (first row) was higher in PD than controls for all regions except the caudate, and the putamen and caudate are differentiated as having low kurtosis (last row). Looking vertically, the differences in diffusivity occurred in the regions of relatively low iron deposition and low kurtosis. Error bars represent 95% confidence interval.

Table 2
Comparison of susceptibility value on QSM between Parkinson's disease patients and healthy controls by means of *t*-test for each region of interest.

Grey nuclei	Mean susceptibility, ppb (SD)		T-value	P-value
	PD	HC		
Globus pallidus	133.71 (60.43)	109.06 (43.91)	−1.50	0.140
Putamen	64.75 (24.39)	44.61 (17.70)	−3.03	**0.004** **
Caudate	35.84 (17.44)	36.81 (17.10)	0.19	0.847
Lateral SN	87.64 (45.17)	77.32 (31.88)	−0.82	0.416
Medial SN	110.32 (56.09)	89.68 (51.90)	−1.26	0.212

PD, Parkinson's Disease; HC, Healthy Controls; SN, substantia nigra; SD, standard deviation.
** $p < 0.005$

Significant group differences in the primary diffusion measure, MD, were also found in the putamen (PD: 1.11, HC: 0.99; $p = 0.013$) and lateral SN (PD: 1.35, HC: 1.21; $p = 0.029$) (Table S1), with the PD group having higher MD, although these did not pass Bonferroni correction. Closer investigation of the secondary measures revealed that the putamen difference followed a similar pattern to that of the caudate, with increased RD ($p = 0.004$) and unchanged AD ($p = 0.238$), and unchanged kurtosis measures except for a reduced KFA ($p = 0.047$). The higher MD in the lateral SN in PD was also driven predominantly by the radial ($p = 0.042$) rather than the axial component, and there were no differences in any other secondary measure. There were no significant differences in either primary or secondary diffusion and kurtosis measures in the GP and medial SN, which were regions with the highest susceptibility value.

3.3. Association with clinical scores

In PD patients, we found a significant direct association between the MDS-UPDRS III score and iron deposition in the putamen (β coefficient = 0.21 [0.08, 0.35], $p = 0.003$) which passed multiple comparison correction (Table 4), as consistent with the significant group difference in susceptibility value in the putamen. We also found significant association between H&Y stage and susceptibility value in the putamen (β coefficient = 0.01 [0.00, 0.02], $p = 0.034$), although this did not pass multiple comparison correction. Last, the MD in the caudate was significantly associated with H&Y stage (β coefficient = 1.09 [0.21, 1.96], $p = 0.016$), but this also was not significant after multiple comparison correction.

We did not find any significant associations between the primary diffusion and kurtosis measures and QSM when controlling for age and sex in any region (Table S2).

Table 4
Linear regression between primary imaging measures (mean susceptibility, MD and MK) and MDS-UPDRS III or H&Y score for each region.

Clinical Motor Measure /Deep Grey Nuclei	β coefficient (95% CI), p-value		
	Mean susceptibility, ppb	MD, $10^{-3}mm^2/s$	MK
MDS-UPDRS III			
Globus pallidus	0.04 (-0.02, 0.10), 0.165	21.92 (-0.43, 44.27), 0.054	−0.20 (-18.29, 17.89), 0.983
Putamen	**0.21 (0.08, 0.35), 0.003** **	15.75 (-5.02, 36.51), 0.134	6.16 (-31.51, 43.83), 0.744
Caudate	−0.07 (-0.28, 0.14), 0.508	8.18 (-6.85, 23.21), 0.280	23.22 (−23.81, 70.24), 0.327
Lateral SN	0.01 (-0.08, 0.09), 0.853	10.46 (-5.83, 26.75), 0.204	−21.19 (-49.45, 7.07), 0.139
Medial SN	0.06 (-0.01, 0.12), 0.071	−7.07 (-31.94, 17.79), 0.571	−2.02 (-20.28, 16.23), 0.825
H&Y			
Globus pallidus	0.00 (0.00, 0.01), 0.229	1.13 (-0.26, 2.51), 0.110	0.38 (-0.73, 1.49), 0.494
Putamen	**0.01 (0.00, 0.02), 0.034** *	1.22 (-0.04, 2.48), 0.058	0.40 (-1.91, 2.72), 0.728
Caudate	−0.01 (-0.02, 0.01), 0.377	**1.09 (0.21, 1.96), 0.016** *	0.50 (-2.39, 3.39), 0.730
Lateral SN	0.00 (0.00, 0.01), 0.658	0.69 (-0.31, 1.68), 0.174	−1.35 (-3.08, 0.38), 0.124
Medial SN	0.00 (0.00, 0.01), 0.267	−0.91 (-2.42, 0.61), 0.235	0.37 (-0.75, 1.49), 0.511

MD, mean diffusivity; MK, mean kurtosis; H&Y, Hoehn & Yahr stage; MDS-UPDRS III, Movement Disorder Society-Unified Parkinson's Disease Rating Scale Part III; SN, substantia nigra.
* $p < 0.05$
** $p < 0.005$

3.4. Composite DKI-QSM biomarker

The marker was formed from the product of the putamen iron, putamen RD, caudate RD and caudate FA, divided by the product of the putamen KFA and the caudate KFA.

$$CompositeDiagnosticMarker = \frac{PutamenQSM \times PutamenRD \times CaudateRD \times CaudateFA}{PutamenKFA \times CaudateKFA}$$

The measurements in the marker above were selected based on whether they had a significant group effect individually and whether they were already closely related to other significant measures. For example, for the putamen, where both the MD and RD were significant individually, only the RD was included in the composite because the MD is already formed from the RD and thus adds minimal unique information. With this approach, we also distinguished "diffusion" from "kurtosis" measures, so FA and KFA would both be included if significant, as

Table 3
Comparison of the deep grey nuclear primary DKI indices between PD and HC groups by independent samples *t*-test.

Deep Grey Nuclei	Mean MD, $10^{-3}mm^2/s$ (SD)		T-value	P-value	Mean MK (SD)		T-value	P-value
	PD	HC			PD	HC		
Globus pallidus	1.292 (0.171)	1.251 (0.117)	−0.88	0.383	1.258 (0.213)	1.242 (0.161)	−0.26	0.795
Putamen	1.105 (0.174)	0.987 (0.141)	−2.63	**0.013** *	0.873 (0.083)	0.874 (0.128)	0.04	0.969
Caudate	1.156 (0.265)	0.957 (0.103)	−4.04	**<0.001** **	0.787 (0.070)	0.780 (0.097)	−0.28	0.778
Lateral SN	1.345 (0.217)	1.206 (0.175)	−2.49	**0.029** *	1.254 (0.126)	1.278 (0.118)	0.64	0.526
Medial SN	1.316 (0.136)	1.348 (0.161)	0.71	0.445	1.306 (0.211)	1.251 (0.133)	−1.19	0.240

PD, Parkinson's Disease; HC, Healthy Controls; SN, substantia nigra; MD, mean diffusivity; MK, mean kurtosis; SD, standard deviation.
* $p < 0.05$
** $p < 0.005$

was the case for the caudate nucleus.

The resulting marker was significantly different between PD and control groups (Mann-Whitney *U* test: U = 494, p < 0.0001) with an area under a curve of 0.88, suggesting a "good" classification performance (Fig. 3). At the optimal cut-point of 53.79 (determined by the Youden method), the sensitivity and specificity were 86% and 71%, respectively.

4. Discussion

Developing new biomarkers to aid in the diagnosis and understanding the mechanisms of early PD is critical. DKI and QSM are both techniques which could contribute information about microstructural pathology in the basal ganglia for complementary assessment in early PD. We found group differences in both susceptibility value and diffusivity of the basal ganglia which also related to motor performance even in early PD patients, and that, together, these differences had value in the classification of early PD patients.

4.1. QSM

Susceptibility value varied widely across the grey nuclei, being highest in the GP and lowest in the caudate (Fig. 2) in all subjects, which corresponded to histochemical values in the literature (Hallgren and Sourander, 1958). We found a trend of greater susceptibility value in PD patients than controls, albeit not statistically significant, and possibly attributed to the early stages of PD in our patient group. Iron contributes to neurodegeneration seen in PD through generating free radicals which cause neuronal death through oxidative stress (Rouault, 2013; Zecca et al., 2004). Iron also induces structural changes and fibrillation of alpha-synuclein, leading to metabolic disturbances in cerebellar granule neurons (Chou et al., 2008; Uversky et al., 2001). Oxidative stress has been found to cause oligodendrocyte apoptosis and demyelination, causing an inflammatory response and leading to infiltration and proliferation of microglia and macrophages and astrogliosis, which may contribute to the selective degeneration of dopaminergic neurons in the nigrostriatal pathway (Lu et al., 2011).

Our results may shed light on the pattern of brain iron deposition,

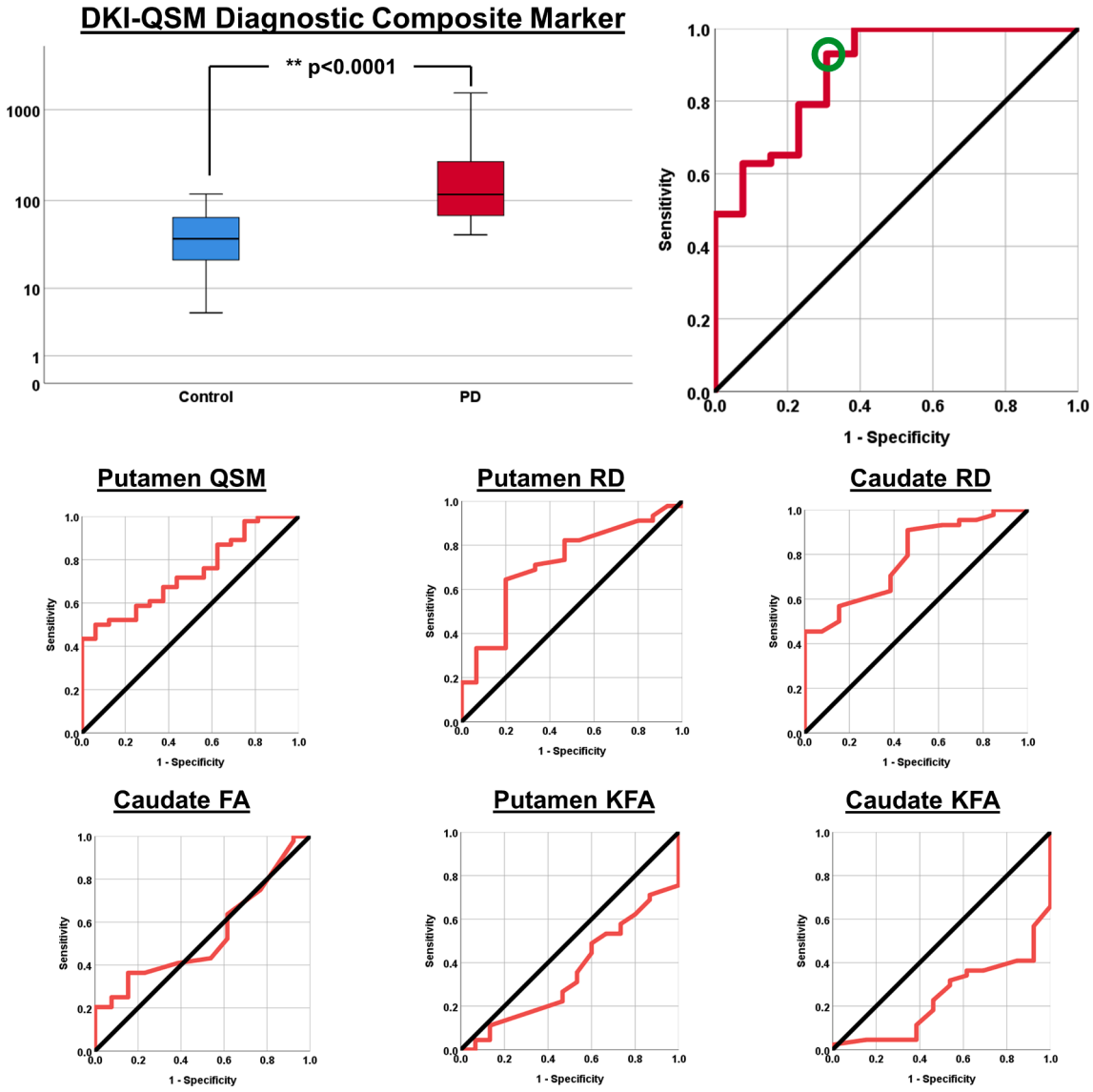

Fig. 3. The combined DKI-QSM composite imaging marker for diagnosis of early PD. Left: Boxplot demonstrating strong significant group difference, whose magnitude surpassed differences in individual measures. Right: Receiver operating characteristic curve for the classification of PD and healthy control groups (red line), demonstrating good classification performance and the optimal cut-point (green circle) where 86% sensitivity and 71% specificity were achieved. Receiver operating characteristic curves of the individual markers (bottom two rows) highlight their relative contribution and improvement achieved in the composite marker.

with iron deposited following the vascular anatomy of the SN and putamen. Histochemical studies have shown ferritin deposits in the neuropil of the vascular network (Morris et al., 1992; Sofic et al., 1991). High iron content can build up in regions related to the venous drainage system, as shown by increase of high iron content in the basal ganglia structures along the venous drainage pathway over time (Liu et al., 2016). Previous studies have also suggested that the build-up of iron in PD patients is a result from the loss of neuromelanin containing dopaminergic neurons. Neuromelanin binds to metals like iron, and hence with progressive increased losses of dopaminergic neurons there will be increased accumulation of iron, leading to neuronal vulnerability from the oxidative damage (Double et al., 2000; Gerlach et al., 2003). While susceptibility value in the putamen is known to increase with age (Ghassaban et al., 2019b; Gong et al., 2015; Hallgren and Sourander, 1958), significant increases in putaminal iron have also been reported in PD on both post-mortem and susceptibility-weighted MRI (Wang et al., 2016; Xuan et al., 2017). Other groups have also reported significantly higher susceptibility values in the SN in PD, while that in other basal ganglia structures did not differ between patients and controls (Ghassaban et al., 2019b; Murakami et al., 2015). These differences may arise from pathophysiologic or methodologic variations in patient recruitment and nuclear segmentation between studies. Further longitudinal studies with standardized automated deep grey nuclear segmentation that fully characterize the progression of spatially differential intranuclear iron deposition in the SN and basal ganglia throughout disease progression in PD would be helpful.

4.2. DKI

MK changes are thought to arise from changes in myelin, axonal and neuronal density, with decreases reflecting mild demyelination, histological changes in neuronal cell bodies, axon and dendrites (Gong et al., 2013), and increases reflecting reactive astrogliosis, microgliosis and increased density of the myelin to cell ratio (Steven et al., 2014). MD is considered to reflect changes in tissue architecture from neuronal loss, vasogenic edema, axonal degeneration and gliosis (Assaf and Pasternak, 2008). Significant increases of MD driven by increase in RD but not accompanied by changes in the DKI indices in the putamen, caudate and lateral SN of PD patients (Table S3) suggest greater cellular loss and injury as the underlying factor.

Our results showed significant increase of FA in the caudate, in congruence with the literature (Atkinson-Clement et al., 2017; Zhang and Burock, 2020). FA is a useful measure of brain connectivity and microstructural diffusion properties. However, the interpretation of changes in FA is not straightforward in grey matter. Damage to grey matter could result in increased gliosis, astrocytic alterations, and other necrotic changes. Such changes could result in a decreased FA because of the increased diffusion direction-potential in the three planes, or in increased FA because of increased structural uniformity secondary to selective neurodegeneration (Stebbins, 2010), such as pruning of the spiny dendrites of striatal neurons which has been reported in post mortem studies and other pathologies (Atkinson-Clement et al., 2017; Villalba and Smith, 2018).

Our results also showed increases of RD in the putamen, caudate and lateral SN of PD patients. An increase in RD was reported to be associated with impaired myelination and may be used as a marker of dysmyelination (Song et al., 2002; Wheeler-Kingshott and Cercignani, 2009). These myelin losses may lead to expansion of the extracellular space, leading to increased degrees of freedom for water diffusion in the orthogonal plane, as reflected in the increase of RD.

4.3. QSM and DKI

Susceptibility value on QSM in the deep grey nuclei were not significantly correlated with DKI indices (Table S2). However, there is suggestion of a trend towards association in the regions of relatively low susceptibility value (putamen and caudate), given the lower p values ($p < 0.1$) for these in Table S2, and congruent with the literature (Gong et al., 2015). The differences in patterns of association between susceptibility value and DKI indices could be explained by the differences in iron content in these areas (Fig. 2). Increased local magnetic susceptibility due to iron may cause signal perturbation in diffusion-weighted images and artefactually alter diffusion indices in caudal iron-rich grey nuclei such as the GP and SN (Rulseh et al., 2013; Surova et al., 2016). Increased iron can reduce the relaxation time and thus substantially reduce signal-to-noise ratio (SNR), masking the effects of DKI (Fig. 2). Thus, a threshold for iron content may exist beyond which diffusion indices would be confounded. In addition, the choice of the diffusion model may also be a factor. Of note, in a histological validation study comparing the single-compartment DKI and the multi-compartment NODDI models in interrogating neuronal density through ferritin content, Gong et al found an association between neuronal density with susceptibility value and NODDI metrics, but not with DKI metrics (Gong et al., 2020).

4.4. Composite DKI-QSM biomarker

Using this approach, the early diagnostic composite marker successfully distinguished early PD from controls with good accuracy at the optimal threshold. This approach integrating diffusion data across regions and imaging modalities has been successful previously in yielding composite markers which relate well to diagnostic status in various neurological diseases (Péran et al., 2010; Welton et al., 2019), but with most studies only incorporating a single modality (Fang et al., 2020; Zhang and Burock, 2020). This is comparable to smaller studies that also showed good classification performance using diffusion metrics (Vaillancourt et al., 2009). This proposed marker should be investigated further in independent early PD cohorts from other centers to test its replicability, especially as there are other studies with different results (Acosta-Cabronero et al., 2017; Vaillancourt et al., 2009). There is also potential in using DKI-QSM to track iron deposition and tissue microstructural integrity in conjunction with clinical disease progression in larger and longitudinal PD cohort studies. Furthermore, the utility of DKI-QSM in distinguishing between subtypes of Parkinsonism early in disease presentation could be further explored, since this is a key diagnostic challenge.

4.5. Limitations

The group ratio between our PD and control groups (approximating 3:1) was not equal in our case-control study. However, both groups were well matched in age ($p = 0.587$) and gender ($p = 0.428$), making our group comparisons valid.

While manual ROI placement had “very good” intra-rater reproducibility and “good” reproducibility between our raters, greater variance across subjects existed for DKI than QSM, especially in the SN, due to its small size, and poorer contrast and resolution of DKI compared to QSM. It is possible that less than precise manual ROI placement could have introduced error into our measurements, albeit efforts were made to exclude CSF and white matter contamination (Zhang and Burock, 2020) using co-registered diffusion and kurtosis maps, and analysis performed only on measurements from Rater 1, who had repeated the entire set of ROI placement for all nuclei, with robust intra-rater reproducibility (ICC > 0.85). Our manual SN ROI approach allowed effective interrogation of quantitative DKI and QSM changes in the caudo-rostrally differential SN cell loss well-known in the literature (Vaillancourt et al., 2009), demonstrating higher MD in the lateral SN ROI in patients than controls, and in keeping with greater dorso-caudal dopaminergic neurodegeneration expected in PD, manifest even in our early PD cohort. Our DKI acquisition could also have been further improved by the addition of more $b = 0$ volumes and isotropic voxels, noteworthy for future longitudinal large cohort study using automated

SN segmentation.

Future work combining DKI and QSM modalities should improve on the approach to apply common regions of interest to both images, which is limited by the differing contrasts, image distortion, resolutions, and lack of default parameters in available imaging registration tools to handle this.

4.6. Conclusion

Our results suggest that QSM and DKI are complementary tools which should be used together for a better understanding of the complex contribution of iron deposition and microstructural changes in the pathophysiology of PD. Future longitudinal studies exploring these changes in disease progression are needed to shed further light on age-related iron accumulation and microstructural changes.

CRediT authorship contribution statement

Samantha Tan: Methodology, Validation, Writing – original draft, Writing – review & editing, Visualization. **Septian Hartono:** Software, Formal analysis, Data curation, Writing – original draft, Visualization. **Thomas Welton:** Methodology, Formal analysis, Writing – review & editing, Visualization. **Ann Chu Ning:** Methodology, Validation, Investigation. **Soo Lee Lim:** Investigation, Resources. **Tong San Koh:** Software. **Huihua Li:** Formal analysis. **Fiona Setiawan:** Investigation. **Samuel Ng:** Investigation. **Nicole Chia:** Investigation. **Saifeng Liu:** Software. **E. Mark Haacke:** Software. **Eng King Tan:** Investigation, Resources, Funding acquisition. **Louis Chew Seng Tan:** Investigation, Funding acquisition. **Ling Ling Chan:** Conceptualization, Methodology, Validation, Investigation, Resources, Writing – review & editing, Visualization, Supervision, Project administration.

Declaration of Competing Interest

The authors declare that they have no known competing financial interests or personal relationships that could have appeared to influence the work reported in this paper.

Acknowledgements

We would like to thank the Singapore National Research Foundation, for their funding support (TCR12dec010) and the excellent team of MR radiographers & physicists for their kind assistance & support in this study. We would also like to thank the team at the Center of Biomedical Imaging, Medical University of South Carolina, and especially Prof Joseph Helpern, for their kind and helpful assistance in using Diffusional Kurtosis Estimator to process the DKI images.

Appendix A. Supplementary data

Supplementary data to this article can be found online at https://doi.org/10.1016/j.nicl.2021.102831.

References

Acosta-Cabronero, J., Cardenas-Blanco, A., Betts, M.J., Butryn, M., Valdes-Herrera, J.P., Galazky, I., Nestor, P.J., 2017. The whole-brain pattern of magnetic susceptibility perturbations in Parkinson's disease. Brain 140 (1), 118–131. https://doi.org/10.1093/brain/aww278.

Alkemade, A., de Hollander, G., Keuken, M.C., Schäfer, A., Ott, D.V.M., Schwarz, J., Weise, D., Kotz, S.A., Forstmann, B.U., Jiang, Q., 2017. Comparison of T2*-weighted and QSM contrasts in Parkinson's disease to visualize the STN with MRI. PLoS One. 12 (4), e0176130. https://doi.org/10.1371/journal.pone.0176130.

Assaf, Y., Pasternak, O., 2008. Diffusion Tensor Imaging (DTI)-based White Matter Mapping in Brain Research: A Review. J Mol Neurosci. 34 (1), 51–61.

Atkinson-Clement, C., Pinto, S., Eusebio, A., Coulon, O., 2017. Diffusion tensor imaging in Parkinson's disease: Review and meta-analysis. Neuroimage Clin. 15 (16), 98–110. https://doi.org/10.1016/j.nicl.2017.07.011.

Azuma, M., Hirai, T., Yamada, K., Yamashita, S., Ando, Y., Tateishi, M., Iryo, Y., Yoneda, T., Kitajima, M., Wang, Y., Yamashita, Y., 2016. Lateral Asymmetry and Spatial Difference of Iron Deposition in the Substantia Nigra of Patients with Parkinson Disease Measured with Quantitative Susceptibility Mapping. AJNR Am J Neuroradiol 37 (5), 782–788. https://doi.org/10.3174/ajnr.a4645.

Barbosa, J.H.O., Santos, A.C., Tumas, V., Liu, M., Zheng, W., Haacke, E.M., Salmon, C.E., 2015. Quantifying brain iron deposition in patients with Parkinson's disease using quantitative susceptibility mapping, R2 and R2*. Magn Reson Imaging. 33 (5), 559–565. https://doi.org/10.1016/j.mri.2015.02.021.

Basser, P.J., Jones, D.K., 2002. Diffusion-tensor MRI: theory, experimental design and data analysis - a technical review. NMR Biomed 15 (7-8), 456–467. https://doi.org/10.1002/(ISSN)1099-149210.1002/nbm.v15:7/810.1002/nbm.783.

Chou, A.P., Maidment, N., Klintenberg, R., Casida, J.E., Li, S., Fitzmaurice, A.G., Fernagut, P.O., Mortazavi, F., Chesselet, M.F., Bronstein, J.M., 2008. Ziram causes dopaminergic cell damage by inhibiting E1 ligase of the proteasome. J Biol Chem. 283 (50), 34696–34703. https://doi.org/10.1074/jbc.m802210200.

Cicchetti, D.V., 1994. Guidelines, criteria, and rules of thumb for evaluating normed and standardized assessment instruments in psychology. Psychological Assessment 6 (4), 284–290. https://doi.org/10.1037/1040-3590.6.4.284.

Damier, P., Hirsch, E.C., Agid, Y., Graybiel, A.M., 1999. The substantia nigra of the human brain. II. Patterns of loss of dopaminergic neurons in Parkinson's disease. Brain 122 (8), 1437–1448. https://doi.org/10.1093/brain/122.8.1437.

Double, K.L., Gerlach, M., Youdim, M.B., Riederer, P., 2000. Impaired iron homeostasis in Parkinson's disease. J Neural Transm Suppl. 60, 37–58. https://doi.org/10.1007/978-3-7091-6301-6_3.

Dusek, P., Jankovic, J., Le, W., 2012. Iron dysregulation in movement disorders. Neurobiol Dis 46 (1), 1–18. https://doi.org/10.1016/j.nbd.2011.12.054.

Dusek, P., Roos, P.M., Litwin, T., Schneider, S.A., Flaten, T.P., Aaseth, J., 2015. The neurotoxicity of iron, copper and manganese in Parkinson's and Wilson's diseases. J Trace Elem Med Biol 31, 193–203. https://doi.org/10.1016/j.jtemb.2014.05.007.

Fang, E., Ann, C.N., Maréchal, B., Lim, J.X., Tan, S.Y.Z., Li, H., Gan, J., Tan, E.K., Chan, L. L., 2020. Differentiating Parkinson's disease motor subtypes using automated volume-based morphometry incorporating white matter and deep gray nuclear lesion load. J Magn Reson Imaging 51 (3), 748–756. https://doi.org/10.1002/jmri.v51.310.1002/jmri.26887.

Gelb, D.J., Oliver, E., Gilman, S., 1999. Diagnostic criteria for Parkinson disease. Archives of Neurology 56 (1), 33–39. https://doi.org/10.1001/archneur.56.1.33.

Gerlach, M., Double, K.L., Ben-Shachar, D., Zecca, L., Youdim, M.B., Riederer, P., 2003. Neuromelanin and its interaction with iron as a potential risk factor for dopaminergic neurodegeneration underlying Parkinson's disease. Neurotox Res. 5 (1–2), 35–44. https://doi.org/10.1007/bf03033371.

Ghassaban, K., Liu, S., Jiang, C., Haacke, E.M., 2019a. Quantifying iron content in magnetic resonance imaging. Neuroimage. 187, 77–92. https://doi.org/10.1016/j.neuroimage.2018.04.047.

Ghassaban, K., He, N., Sethi, S.K., Huang, P., Chen, S., Yan, F., Haacke, E.M., 2019b. Regional High Iron in the Substantia Nigra Differentiates Parkinson's Disease Patients From Healthy Controls. Front Aging Neurosci. 11, 106. https://doi.org/10.3389/fnagi.2019.00106.

Gong, N.J., Wong, C.S., Chan, C.C., Leung, L.M., Chu, Y.C., 2013. Correlations between microstructural alterations and severity of cognitive deficiency in Alzheimer's disease and mild cognitive impairment: A diffusional kurtosis imaging study. Magn Reson Imaging 31 (5), 688–694. https://doi.org/10.1016/j.mri.2012.10.027.

Gong, N.J., Wong, C.S., Hui, E.S., Chan, C.C., Leung, L.M., 2015. Hemisphere, gender and age-related effects on iron deposition in deep gray matter revealed by quantitative susceptibility mapping. NMR Biomed. 28 (10), 1267–1274. https://doi.org/10.1002/nbm.3366.

Gong, N.J., Dibb, R., Pletnikov, M., Benner, E., Liu, C., 2020. Imaging microstructure with diffusion and susceptibility MR: neuronal density correlation in Disrupted-in-Schizophrenia-1 mutant mice. NMR Biomed. 33 (10), e4365 https://doi.org/10.1002/nbm.4365.

Griffiths, P.D., Crossman, A.R., 1993. Distribution of iron in the basal ganglia and neocortex in postmortem tissue in Parkinson's disease and Alzheimer's disease. Dementia. 4 (2), 61–65. https://doi.org/10.1159/000107298.

Haacke, E.M., Tang, J., Neelavalli, J., Cheng, Y.C.N., 2010. Susceptibility mapping as a means to visualize veins and quantify oxygen saturation. J Magn Reson Imaging. 32 (3), 663–676. https://doi.org/10.1002/jmri.v32:310.1002/jmri.22276.

Hallgren, B., Sourander, P., 1958. The effect of age on the non-haemin iron in the human brain. J Neurochem. 3 (1), 41–51. https://doi.org/10.1111/jnc.1958.3.issue-110.1111/j.1471-4159.1958.tb12607.x.

Huang, X., Ng, S.Y.E., Chia, N.S.Y., Setiawan, F., Tay, K.Y., Au, W.L., Tan, E.K., Tan, L.C. S., 2019. Non-motor symptoms in early Parkinson's disease with different motor subtypes and their associations with quality of life. Eur J Neurol 26 (3), 400–406. https://doi.org/10.1111/ene.13803.

Hughes, A.J., Daniel, S.E., Ben-Shlomo, Y., Lees, A.J., 2002. The accuracy of diagnosis of parkinsonian syndromes in a specialist movement disorder service. Brain 125 (4), 861–870. https://doi.org/10.1093/brain/awf080.

Langkammer, C., Schweser, F., Krebs, N., Deistung, A., Goessler, W., Scheurer, E., Sommer, K., Reishofer, G., Yen, K., Fazekas, F., Ropele, S., Reichenbach, J.R., 2012. Quantitative susceptibility mapping (QSM) as a means to measure brain iron? A post mortem validation study. Neuroimage. 62 (3), 1593–1599. https://doi.org/10.1016/j.neuroimage.2012.05.049.

Liu, M., Liu, S., Ghassaban, K., Zheng, W., Dicicco, D., Miao, Y., Habib, C., Jazmati, T., Haacke, E.M., 2016. Assessing global and regional iron content in deep gray matter as a function of age using susceptibility mapping. J Magn Reson Imaging. 44 (1), 59–71. https://doi.org/10.1002/jmri.25130.

Lu, H., Jensen, J.H., Ramani, A., Helpern, J.A., 2006. Three-dimensional characterization of non-gaussian water diffusion in humans using diffusion kurtosis imaging. NMR Biomed 19 (2), 236–247. https://doi.org/10.1002/(ISSN)1099-149210.1002/nbm.v19:210.1002/nbm.1020.

Lu, Z., Jiang, H., Xu, H., Song, N., Xie, J., 2011. Increased iron levels correlate with the selective nigral dopaminergic neuron degeneration in Parkinson's disease. J Neural Transm. 118 (3), 361–369. https://doi.org/10.1007/s00702-010-0434-3.

Morris, C.M., Candy, J.M., Oakley, A.E., Bloxham, C.A., Edwardson, J.A., 1992. Histochemical distribution of non-haem iron in the human brain. Acta Anatomica 144 (3), 235–257. https://doi.org/10.1159/000147312.

Murakami, Y., Kakeda, S., Watanabe, K., Ueda, I., Ogasawara, A., Moriya, J., Ide, S., Futatsuya, K., Sato, T., Okada, K., Uozumi, T., Tsuji, S., Liu, T., Wang, Y., Korogi, Y., 2015. Usefulness of quantitative susceptibility mapping for the diagnosis of Parkinson disease. AJNR Am J Neuroradiol. 36 (6), 1102–1108. https://doi.org/10.3174/ajnr.a4260.

Péran, P., Cherubini, A., Assogna, F., Piras, F., Quattrocchi, C., Peppe, A., Celsis, P., Rascol, O., Démonet, J.F., Stefani, A., Pierantozzi, M., Pontieri, F.E., Caltagirone, C., Spalletta, G., Sabatini, U., 2010. Magnetic resonance imaging markers of Parkinson's disease nigrostriatal signature. Brain 133 (11), 3423–3433. https://doi.org/10.1093/brain/awq212.

Rouault, T.A., 2013. Iron metabolism in the CNS: implications for neurodegenerative diseases. Nat Rev Neurosci 14 (8), 551–564. https://doi.org/10.1038/nrn3453.

Rulseh, A.M., Keller, J., Tintěra, J., Kožíšek, M., Vymazal, J., 2013. Chasing shadows: what determines DTI metrics in gray matter regions? An in vitro and in vivo study. J Magn Reson Imaging. 38 (5), 1103–1110. https://doi.org/10.1002/jmri.24065.

Sethi, S.K., Kisch, S.J., Ghassaban, K., Rajput, A., Rajput, A., Babyn, P.S., Liu, S., Szkup, P., Mark Haacke, E., 2019. Iron quantification in Parkinson's disease using an age-based threshold on susceptibility maps: The advantage of local versus entire structure iron content measurements. Magn Reson Imaging. 55, 145–152. https://doi.org/10.1016/j.mri.2018.10.001.

Sian-Hülsmann, J., Mandel, S., Youdim, M.B.H., Riederer, P., 2011. The relevance of iron in the pathogenesis of Parkinson's disease. J Neurochem 118 (6), 939–957. https://doi.org/10.1111/j.1471-4159.2010.07132.x.

Sofic, E., Paulus, W., Jellinger, K., Riederer, P., Youdim, M.B.H., 1991. Selective increase of iron in substantia nigra zona compacta in Parkinsonian brains. J Neurochem. 56 (3), 978–982. https://doi.org/10.1111/j.1471-4159.1991.tb02017.x.

Song, S.K., Sun, S.W., Ramsbottom, M.J., Chang, C., Russell, J., Cross, A.H., 2002. Dysmyelination revealed through MRI as increased radial (but unchanged axial) diffusion of water. Neuroimage. 17 (3), 1429–1436. https://doi.org/10.1006/nimg.2002.1267.

Stebbins, G.T., 2010. In: Encyclopedia of Movement Disorders. Elsevier, pp. 308–310. https://doi.org/10.1016/B978-0-12-374105-9.00020-4.

Stebbins, G.T., Goetz, C.G., Burn, D.J., Jankovic, J., Khoo, T.K., Tilley, B.C., 2013. How to identify tremor dominant and postural instability/gait difficulty groups with the movement disorder society unified Parkinson's disease rating scale: comparison with the unified Parkinson's disease rating scale. Mov Disord. 28 (5), 668–670. https://doi.org/10.1002/mds.25383.

Steven, A.J., Zhuo, J., Melhem, E.R., Aj, S., Zhuo, J., Er, M., 2014. Diffusion Kurtosis Imaging: An Emerging Technique for Evaluating the Microstructural Environment of the Brain. AJR Am J Roentgenol. 202 (1), 26–33. https://doi.org/10.2214/ajr.13.11365.

Surova, Y., Lampinen, B., Nilsson, M., Lätt, J., Hall, S., Widner, H., van Westen, D., Hansson, O., Leemans, A., 2016. Alterations of Diffusion Kurtosis and Neurite Density Measures in Deep Grey Matter and White Matter in Parkinson's Disease. PLoS One. 11 (6), e0157755. https://doi.org/10.1371/journal.pone.0157755.

Tabesh, A., Jensen, J.H., Ardekani, B.A., Helpern, J.A., 2011. Estimation of tensors and tensor-derived measures in diffusional kurtosis imaging. Mag Reson Med. 65 (3), 823–836. https://doi.org/10.1002/mrm.22655.

Uversky, V.N., Li, J., Fink, A.L., 2001. Metal-triggered structural transformations, aggregation, and fibrillation of human alpha-synuclein. A possible molecular NK between Parkinson's disease and heavy metal exposure. J Biol Chem. 276 (47), 44284–44296. https://doi.org/10.1074/jbc.m105343200.

Vaillancourt, D.E., Spraker, M.B., Prodoehl, J., Abraham, I., Corcos, D.M., Zhou, X.J., Comella, C.L., Little, D.M., 2009. High-resolution diffusion tensor imaging in the substantia nigra of de novo Parkinson disease. Neurology. 72 (16), 1378–1384. https://doi.org/10.1212/01.wnl.0000340982.01727.6e.

Villalba, R.M., Smith, Y., 2018. Loss and remodeling of striatal dendritic spines in Parkinson's disease: from homeostasis to maladaptive plasticity? J Neural Transm (Vienna). 125 (3), 431–447. https://doi.org/10.1007/s00702-017-1735-6.

Wang, J.J., Lin, W.Y., Lu, C.S., Weng, Y.H., Ng, S.H., Wang, C.H., Liu, H.L., Hsieh, R.H., Wan, Y.L., Wai, Y.Y., 2011. Parkinson Disease: Diagnostic Utility of Diffusion Kurtosis Imaging. Radiology. 261 (1), 210–217. https://doi.org/10.1148/radiol.11102277.

Wang, Y., Liu, T., 2015. Quantitative susceptibility mapping (QSM): Decoding MRI data for a tissue magnetic biomarker. Magn Reson Med. 73 (1), 82–101. https://doi.org/10.1002/mrm.25358.

Wang, J.Y., Zhuang, Q.Q., Zhu, L.B., Zhu, H., Li, T., Li, R., Chen, S.-F., Huang, C.-P., Zhang, X., Zhu, J.-H., 2016. Meta-analysis of brain iron levels of Parkinson's disease patients determined by postmortem and MRI measurements. Sci Rep. 6, 36669. https://doi.org/10.1038/srep36669.

Welton, T., Maller, J.J., Lebel, R.M., Tan, E.T., Rowe, D.B., Grieve, S.M., 2019. Diffusion kurtosis and quantitative susceptibility mapping MRI are sensitive to structural abnormalities in amyotrophic lateral sclerosis. Neuroimage Clin. 24, 101953. https://doi.org/10.1016/j.nicl.2019.101953.

Wheeler-Kingshott, C.A.M., Cercignani, M., 2009. About "axial" and "radial" diffusivities. Magn Reson Med. 61 (5), 1255–1260. https://doi.org/10.1002/mrm.v61:510.1002/mrm.21965.

Xuan, M., Guan, X., Gu, Q., Shen, Z., Yu, X., Qiu, T., Luo, X., Song, R., Jiaerken, Y., Xu, X., Huang, P., Luo, W., Zhang, M., 2017. Different iron deposition patterns in early- and middle-late-onset Parkinson's disease. Parkinsonism Relat Disord. 44, 23–27. https://doi.org/10.1016/j.parkreldis.2017.08.013.

Zecca, L., Youdim, M.B.H., Riederer, P., Connor, J.R., Crichton, R.R., 2004. Iron, brain ageing and neurodegenerative disorders. Nat Rev Neurosci. 5 (11), 863–873. https://doi.org/10.1038/nrn1537.

Zhang, G., Zhang, Y., Zhang, C., Wang, Y., Ma, G., Nie, K., Xie, H., Liu, J., Wang, L., 2015. Diffusion Kurtosis Imaging of Substantia Nigra Is a Sensitive Method for Early Diagnosis and Disease Evaluation in Parkinson's Disease. Parkinsons Dis. 2015, 1–5. https://doi.org/10.1155/2015/207624.

Zhang, Y., Burock, M.A., 2020. Diffusion Tensor Imaging in Parkinson's Disease and Parkinsonian Syndrome: A Systematic Review. Front Neurol. 25 (11), 531993 https://doi.org/10.3389/fneur.2020.531993.